DESIGN AND ANALYSIS OF MULTI-CAVITY TRADITIONAL AND H-BRANCHING RUNNERS FOR PLASTIC INJECTION MOLD

(Date received: 20.11.2007)

Mohd. Rizwan Hamsin, Azuddin Mamat and Aznijar Ahmad-Yazid
Department of Engineering Design and Manufacture
Faculty of Engineering, University of Malaya,
50603, UM, Kuala Lumpur
E-mail: aznijar@um.edu.my

ABSTRACT

This paper describes the design and analysis of plastic injection mold balancing runner. The runners were designed based on Ellis Model, a viscosity model of flow network consisting of elements and nodes. 4-coefficients viscosity model and temperature dependence Ellis Model were used in order to reduce the amount of computational analysis by FEA software. A Cross WLF viscosity model was used in the FEA analysis. FEA simulation of injection molding was conducted for 8 and 16 cavity runners. Runner layout was assumed as pressure at the end of each element acting as an initial and final boundary condition. The length and size of the runner can be adjusted to fit the boundary condition that had been chosen. Flow rates at each element leading to gates were set to simulate the desired pressure drop. The final boundary condition for the first element was set as the initial boundary condition for the next element. By employing Ellis model, it was shown that the calculated results are similar to the result obtained through simulation. The model employed has successfully shown an equal filling time for each cavity, an equal pressure at each gate as well as uniform part filling. A predictive FEA performed prior to actual manufacturing is helpful in order to produce good molds.

Keywords: *Ellis Model, Flow Analysis, Plastic Injection Mold, Runner Design, Simulation*

1.0 INTRODUCTION

Injection molding is one of the most important manufacturing processes in the industry. It leads to a higher manufacturing rate, shorter product cycle and low percentage of scrap, excellent product surface and easy molding of complicated shapes [1]. An important aspect in good injection molding process is the runner and gating system design. The main function of runner and gating system is to deliver molten plastic into the mould through all sections of the mold cavities. Poor runner and gating design can lead to defects such as gas porosity, shrinkage porosity, flow line cold shut, and poor surface quality. With good runner and gating design, one may control the filling pattern and prevents over-packing. Incidences of faulty molded parts can be reduced, hence increasing productivity.

A runner is defined as an at least one-dimensional element that connects two nodes. In most cases, the elements within a runner have constant diameter. However, if the diameters vary, re-sizing will be performed proportionally. Demands for tighter tolerances, near-zero reject, and ever-lower costs that were once limited to automotive and medical jobs are now required even for molders of common consumer product. Molders have often responded by limiting themselves to molds of low cavities because they are the easiest way to balance naturally. But the use of low cavities molds would result in the increase of the numbers of molds, using more machines. This eventually results in an increase of floor space for the machines and people. However, to remain competitive in a global marketplace, cost can only be reduced by producing parts faster consistently and reduce the number of scrap. Hitherto, the importance of runner analysis on design and molding seems to have been long overlooked. Many flow analyses have been conducted, but the focus tends to be mainly on the part and cavity. However, many researchers have indicated that the runners play a much more significant role than many might realise [2, 3, 4].

Zhao *et al.* [5] performed numerical simulations on coupled fluid flow and heat transfer in a thin liquid slag or flux layer. Steady state Navier–Stokes equations were solved using a commercial finite volume software, FLUENT. The combined effects of natural convection, bottom shear velocity and strongly temperature dependent viscosity were investigated.

Lee and Lin *et al*. [6] designed a runner and gating system for a multi-cavity injection mould using Finite Element Method (FEM) and neural network. In order to select the optimal runner system parameter to minimise the warp of an injection mould, FEM, Taguchi's method and an adductive network were used. A satisfactory result as compared to the corresponding finite element verification was obtained. Fan *et al*. [7] studied real time flow rate estimation in injection molding. Experimental and analytical

methods were employed in this study in order to estimate the flow rate and pressure at multiple points in an injection mold. In the experiments, melt pressure transducers were positioned at the inlet and the outlets of the feed system. A non-Newtonian, non-isothermal, faster than real time simulation utilised the feedback from the experiments to estimate the flow rates delivered through each branch of the feed system, and also provided feedback with regards to the apparent viscosity of the polymer melt provided by the molding machine. A two-cavity mold with a valve-gated hot runner system was studied.

Kumar *et. al*. [8] performed a computer simulation for the transport processes during an injection mold filling and managed to optimise the molding condition. The computer simulation of injection mold filling at constant flow rate was modeled for the production of a cylindrical part under isothermal and non-isothermal conditions. The finite difference method used to solve the governing differential equation for both the processes yield good agreement with the analytical solutions.

Plastics injection molding has been limited by the lack of observability and controllability, such that it is impossible to identify or control flow rates and pressures at multiple locations of a mold. An analysis method is available to estimate the flow rate and pressure at multiple points in an injection mold. Poorly designed runner systems are often the main cause for many molding issues that could be solved by re-designing/modifying the runners without making any changes to other parts of the mold.

The research aims to investigate the feasibility of adopting a simulation, in this case, MoldFlow software, during a mold design exercise, rather than to keep on relying on trial and error technique currently used. By using two different runner configurations, it is also desired to identify the appropriate runner system to be adopted in order to achieve best flow-rate within the runners. In the following sections of this paper, the design and analysis of traditional and h-branching runners for plastic injection mold are explained in detail and the results obtained are discussed.

2.0 NUMERICAL BACKGROUND

To model the injection mold runner, a viscosity models for flow analysis function is required. A number of well known models such as Power law models, Carreau model, Cross model and Ellis model are available. The aim in employing a viscosity model is to match the observed behavior of the material as closely as possible.

2.1 ELLIS MODEL

For this work, an Ellis model is used. The runner system in injection mold is modeled as a flow network, consists of elements and nodes. Each element consists of cylindrical elements of unknown lengths and diameter. An Ellis model in terms of shear rate is written as follows:

$$\left(\frac{\eta_0}{\eta} = 1 + \frac{\tau}{\tau_{\frac{1}{2}}}\right)^{\alpha-1} \tag{1}$$

where $\tau_{1/2}$ is the shear stress at which the viscosity is 50% of the Newtonian limit, η_0 , and α-1 is the slope of the viscosity in the power law regime. For the purpose of modeling the temperature dependence of the rheology, the zero shear rate viscosity is modeled with Arrhenius type dependence as:

$$\pi_0 = \mu \exp(T) \tag{2}$$

Where, T is temperature from previous time step.

2.2 DERIVATION FOR RODS

Considering the viscous flow in a rod with an open end, the relationship between flow rate and pressure gradient can be assumed as:

$$Q = \frac{\pi R^4 - \Delta P}{8\eta L}\left[1 + \left(\frac{R\Delta P}{2L\tau_{\frac{1}{2}}}\right)^{\alpha-1}\right] \tag{3}$$

where Q is the volumetric flow rate, R is the rod radius, ΔP is the pressure drop, L is the length of the rod, and other coefficients are from the Ellis model fitting. The shear stress, τ , and shear rate, $\dot{\gamma}$, are, respectively:

$$\tau = \left(\frac{\Delta PR}{2L}\right) \tag{4}$$

$$\dot{\gamma} = \frac{\Delta PR}{2\eta_0 L}\left[1 + \left(\frac{R\Delta P}{2L\tau_{\frac{1}{2}}}\right)^{\alpha-1}\right] \tag{5}$$

For bulk temperature, integrating the shear heating across the radius leads to,

$$P_{x\dot{\gamma}} = 2\pi L\int_0^R \tau\dot{\gamma}RdR = \pi L\left(\frac{\Delta P}{L}\right)^2\frac{R^4}{8\eta_0} + \pi L\left(\frac{\Delta P}{L}\right)^{\alpha+1}\frac{\left(2\tau_{\frac{1}{2}}\right)^{1-\alpha}}{2(\alpha+3)\eta_0} \tag{6}$$

2.3 BOUNDARY CONDITION

With a constant mold wall boundary condition instead of a Biot boundary condition, the transient temperature distribution after a time step Δt is solved as:

$$\frac{T(R,t) - T_{wall}}{T_{melt} - T_{wall}} = \sum_{x=0}^{\infty}\frac{2J_0(\beta_n r)}{(\beta_n R)J_1(\beta_n R)}\exp(-\beta_n^2\Delta ta) \tag{7}$$

where,

T_{melt} The heat conduction between polymers melt with an initial temperature.

T_{wall} Temperature at walls of a cylindrical feed system. a is the thermal diffusivity of the polymer melt. J_0 and J_1 are Bessel functions and β_n is the eigen value. The bulk temperature of the polymer melt, $\bar{T}$, can be estimated as:

$$\frac{\bar{T} - T_{wall}}{T_{melt} - T_{wall}} = \sum_{x=0}^{\infty}\frac{2}{(\beta_n R)J_1(\beta_n R)}\exp(-\beta_n^2\Delta ta)\frac{2\pi\int_0^R J_0(\beta_n r)rdr}{\pi R^2}$$

$$= \sum_{x=0}^{\infty}\frac{4}{(\beta_n R)_2}\exp(-\beta_n^2\Delta ta) \tag{8}$$

Neglecting higher order terms and applying the boundary condition for cylinders, where,

$$\beta_n R \cong \frac{3\pi}{4} \tag{9}$$

Therefore,

$$\bar{T} - T_{wall} = T_{melt} - T_{wall}\left(\frac{64}{9\pi^2}\right)\exp\left(\frac{\frac{-9}{16}\pi^2 a\Delta t}{R^2}\right) \tag{10}$$

This equation does not include the effect of temperature rise due to viscous heating by melting plastic. In order to take into account of viscous heating, the temperature rise due to viscous heating is:

$$\rho C_p \frac{\Delta \bar{T}}{\Delta t} = \frac{P_{xy}}{V} = \left(\frac{\Delta PR}{L}\right)^2 \frac{1}{8\eta_0} + \left(\frac{2\tau_{\frac{1}{2}}}{2(\alpha+3)\eta_0}\right) \tag{11}$$

Effect of viscous heating will indicates that the change in the bulk temperature is:

$$\Delta \bar{T}\frac{\Delta T}{\rho C_p} = \left[\left(\frac{\Delta PR}{L}\right)^2 \frac{1}{8\eta_0} + \frac{\Delta PR}{L}^{\alpha+1} \frac{(2\tau_{\frac{1}{2}})^{1-\alpha}}{2(\alpha+3)\eta_0}\right] \tag{12}$$

It can be concluded that, bulk temperature of a plastic flow with Ellis viscosity model for flow in a rod, taking into viscous heating and heat conduction with an estimated pressure drop is:

$$\bar{T} = T_{wall} + (T_{melt} - T_{wall})\frac{64}{9\pi^2}\exp\left(\frac{\frac{-9}{16}\pi^2 a\Delta t}{R^2}\right) + \frac{\Delta t}{\rho C_p}$$
$$\left[\left(\frac{\Delta PR^2}{L}\right)\frac{1}{8\eta_0} + \left(\frac{\Delta PR}{L}\right)^{\alpha+1}\left(\frac{(2\tau_{\frac{1}{2}})^{1-\alpha}}{2(\alpha+3)\eta_0}\right)\right] \tag{13}$$

3.0 RESEARCH DESIGN

This section explains in details, the runner size, runner layout, processing condition, boundary condition and rules of estimation used in this work. Figure 1 shows the research design flow chart that was followed.

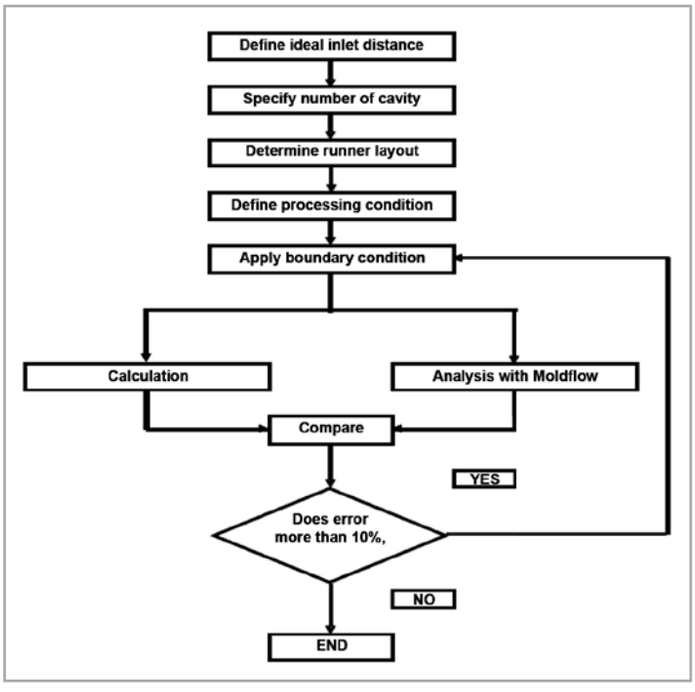

Figure 1 : Research design flow chart

3.1 RUNNER DIAMETER AND LENGTH ESTIMATION

The purpose of this technique is to control the pressure and flow rate in runner elements. This is performed by estimating the pressure drop within an element, the end pressure at gates and achieving equal flow rate at each runner approaching to gate. Consider part shown in Figure 2.

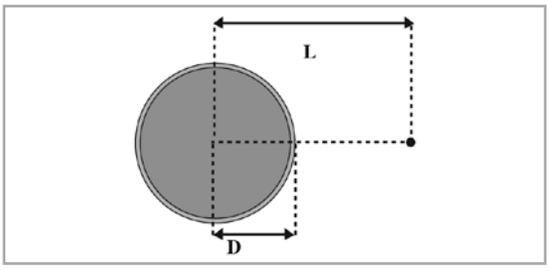

Figure 2 : Estimation of length from inlet to 1st branch

From element 1, taken as starting point, the ideal distance, *L* between injection points parallel to inlet is determined. This is known as length of the first element. Assuming at inlet, plastic flow is injected with 6 MPa at melt temperature of 230°C. Molten plastic will flow from position 0 to position 1 in 0.5 sec. Note that position 0 is inlet, and position 1 is 1st. branch. At 1st. branch, the assumed pressure is at 5.5MPa. Thus, flow rate across element 1 and bulk temperature can be calculated. But, these values can be adjusted by changing the radius of runner. For the first element, these values are taken. Since 1st. branch leads to elements 2, 3 and 4, final condition of element 1 will be used as initial condition for elements 2, 3 and 4. Between elements 2 and 3, only element 2 will be used to analyzes the flow condition because both elements have similar length and radius. Therefore, flow in element 2, pressure at final condition is assumed to be equal to all gate entrance. For that reason, a proper value must be selected to avoid too large or too small pressure drop in other element.

3.2 RUNNER LAYOUT AND CONFIGURATION

A technique to calculate desired length and radius of a runner is already available. By following Kazmer method [9], the entire runner network layout was modeled as a flow network, consists of elements and nodes. For research purpose, a traditional and H-branching will be used. Since this layout is symmetrical, analysis will be taken on the half side of the runner, with assumption that melt will flow equally to the other half. Also, on the half side, analysis will be performed on the lower half of the runner. For example, Figure 3 shows a numbered elements and nodal used for the analysis in a typical 8 cavity runner layout. Therefore, elements that will be observed are elements 1, 2, 4 and 5. The elements 2 and 5, which lead to the gate will be used as comparison. This current work is focused on 8 and 16 cavity for traditional and *H*-branching runner layout.

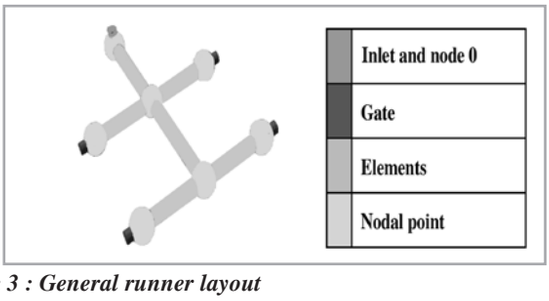

Figure 3 : General runner layout

3.3 PROCESSING CONDITION

Processing condition should satisfy Equations (3) and (13). Material used is polypropylene. The material constant can be obtained from experimental process using viscometer, fitting the Ellis model to material data or the Cross-WLF model database from MoldFlow [6]. For this work, the coefficient is chosen by fitting the Ellis model to the material data in Moldflow Database. The properties are shown below:

a	Mold surface temperature	40°C
b	Mold temperature	60°C
c	Melt temperature	240°C
d	Mu	9980 Pa-S
e	Specific heat	2740J/Kg-C
f	Thermal conductivity	0.164 W/m-C
g	Density	775Kg/m^3
h	Material diffusivity	7.72 x 10-8
i	Tau1/2	24200 Pa.s
j	Temperature constant	0.01564 1/C
k	Alpha	2.54
l	Wall temperature	230°C
m	Filling time	Depended on estimated value obtained through the estimated parameter table

3.4 BOUNDARY CONDITION

Each element was then analysed as a symmetrical cylindrical shape. The cylinder is divided into *n* number of sub elements. The number of sub elements depends on the length of the element and mesh size. Boundary conditions were set up at each end of the element. The desired parameters were pressure, temperature and plastic flow rate. Figure 4 shows plastic flow from positions 0 to 1 at a time step Δt.

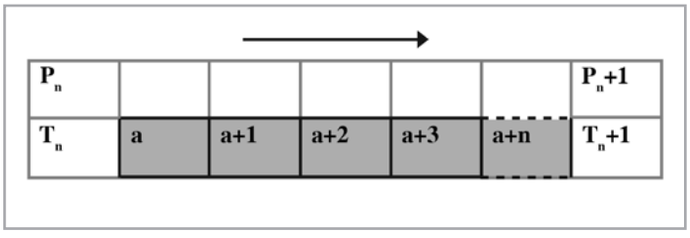

Figure 4 : Element 1 boundary conditions

Pressure drop can be defined by:

$$\Delta p = P_n - P_n{+}1 \tag{14}$$

Temperature is defined by:

$$\Delta T = T_n - T_n{+}1 \tag{15}$$

Equation (3.11) with coefficient from Ellis Model fitting is used to find the bulk temperature at T_n+1. Melt flow rate, Q between n and n+1 is define by using equation (3). Length, L and radius, R is selected randomly, according to size of part. Temperature dependence viscosity, can be defined by

$$\eta_{n+1} = \mu \exp(CT_n) \tag{16}$$

Figure 5 shows an example of boundary condition used for a traditional runner and Figure 6, for an *H*-branching runner.

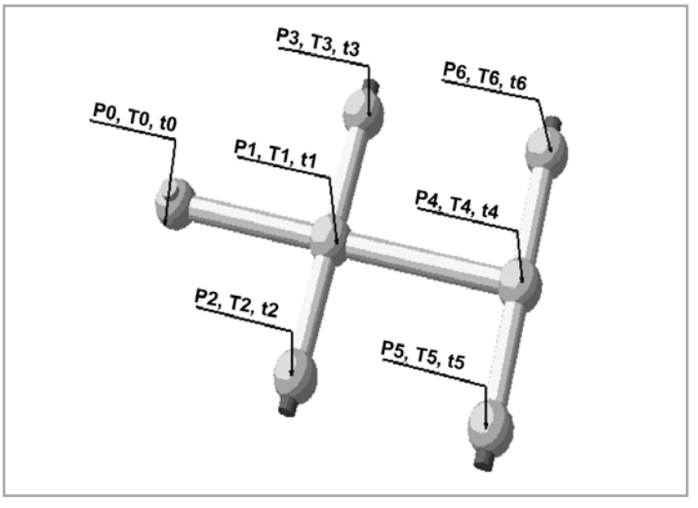

Figure 5 : Boundary condition for traditional runner

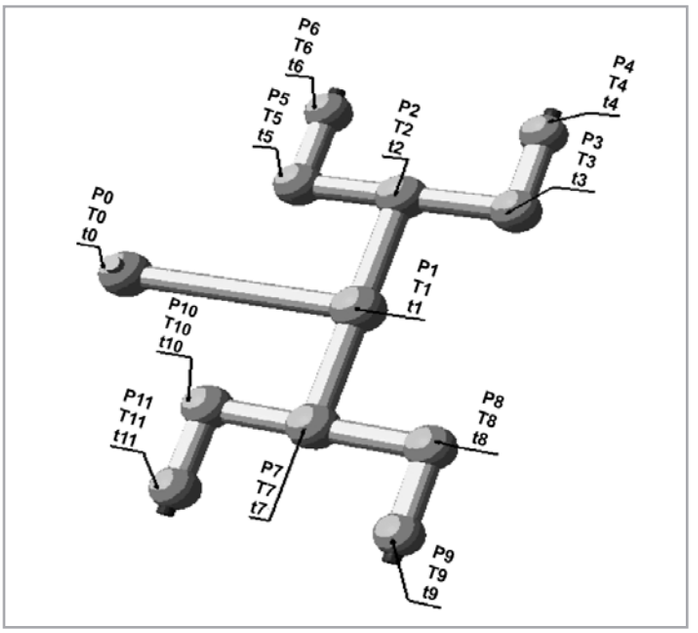

Figure 6 : Boundary condition for H-branching runner

3.5 RULES OF ESTIMATION

The estimation process of each boundary condition to achieve certain desired runner length and diameter is governed by flow rate and pressure distribution. In order to complete the equation, melt flow rate and pressure distribution need to be known. Figure 7 shows an example of the estimated condition for melt flow rate and pressure drop used for traditional runner while Figure 8 is for an *H*-branching runner. The color-shaded area represent elements and nodal in runner layout.

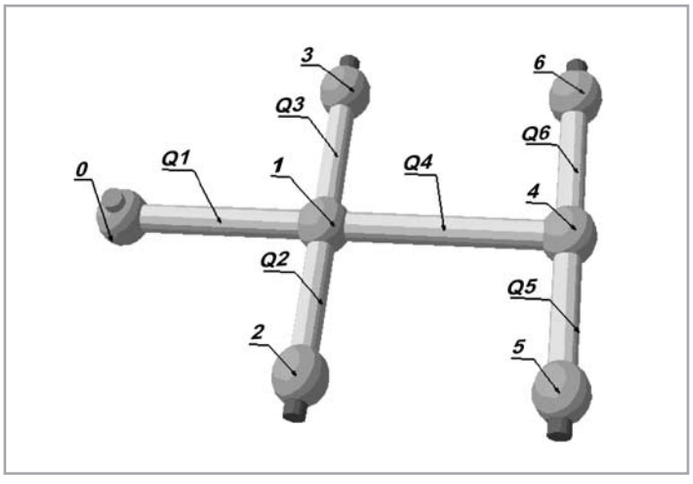

Figure 7 : Melt flow rate distribution for 8 cavity traditional runner

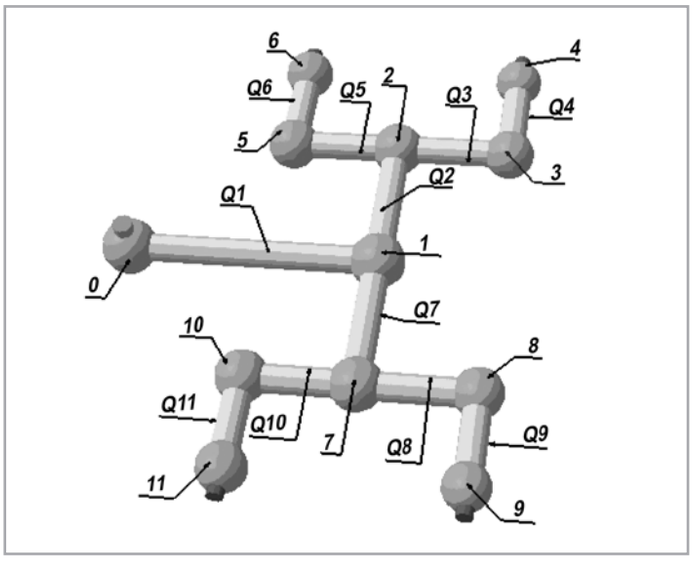

Figure 8 : Melt flow rate distribution for 16 cavity H-branching runner

For traditional runner layout, the melt flow rate;

$$Q_1 \approx 2Q_4 + Q_2 + Q_3 \tag{17}$$

$$Q_1 \approx 4Q_2 \approx 4Q_3 \approx 4Q_5 \approx 4Q_6 \tag{18}$$

Meanwhile, for H type runner layout, the melt flow rate;

$$Q_1 \approx 4Q_2 \approx 8Q_3 \tag{19}$$

$$Q_3 \approx Q_4 \approx Q_5 \approx Q_6 \tag{20}$$

Pressure at each nodal entrance to cavity, must equal approximately

For traditional runner layout, the pressure is approximated,

$$P_2 \approx P_3 \approx P_5 \approx P_6 \tag{21}$$

Meanwhile, for H type runner layout, the pressures,

$$P_4 = P_6 \tag{22}$$

4.0 RESULTS AND DISCUSSIONS

Results obtained through simulation using a Cross-WLF model were compared with the calculation performed based on modified Ellis model. The results are divided into 4 sections: 8 cavities traditional runner, 16 cavities traditional runner, 8 cavities *H*-branching runner and 16 cavities *H*-branching runner and represented in various tables and figures.

4.1 RESULTS FOR 8 CAVITIES TRADITIONAL RUNNER

4.1.1 SIMULATION FOR 8 CAVITY RUNNER

Figure 9 shows a half side layout for 8 cavity traditional runner. The runner layout with numbered flow rate in each element and nodal points is also shown.

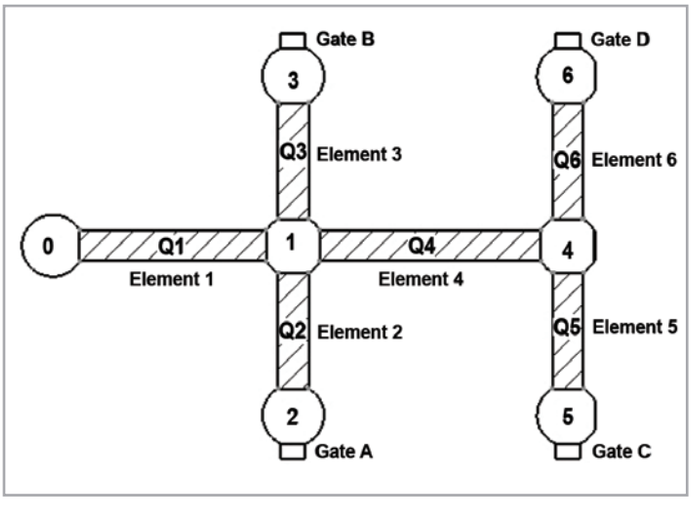

Figure 9 : Half side layout for 8 cavity traditional runner

Table 1 shows the estimated parameters that have been calculated. The first and second rows, represent the initial pressure and the final pressure at each element. In pressure flow path, it is found that one of the cavity exhibit lower pressure at the end of the filling process. In temperature and fill time flow path, all cavities show equal capacity.

Table 1: Parameters for 8 cavity traditional runner

	Elements			
	1	**2**	**4**	**5**
$P_{initial}$ (MPa)	4.00	3.50	3.50	3.00
P_{final} (MPa)	3.50	2.50	3.00	2.50
P_{drop} (MPa)	0.50	1.00	0.50	0.50
Radius (m)	0.0055	0.0037	0.0059	0.0049
Length (m)	0.03	0.03	0.05	0.03
$T_{initial}$ (°C)	240.00	235.94	235.94	232.50
T_{final} (°C)	235.94	239.00	232.50	232.67
Time step (sec)	0.500	0.500	0.500	0.500

Mesh size (m)	0.008	0.008	0.008	0.008
No. of element	3.750	3.750	6.250	3.750
Element time-step	0.133	0.133	0.080	0.133
η (°C)	233.864	249.176	249.176	262.962
Flow rate (m^3/s)	7.505E-05	3.986E-05	3.780E-05	3.753E-05
Flow rate (cc/s)	75.051	39.864	37.802	37.535

4.1.2 MELT FLOW PATH FOR 8 CAVITY RUNNER

Result of fill time for traditional 8 cavity runner shown in Figure 10, with the pressure distribution plot shown in Figure 11, and the temperature distribution plot in Figure 12.

Similar-colored plots shown in Figures 10, 11 and 12 indicated an equal fill time, pressure and temperature at each gate. Comparisons of the pressure drops for 8 cavity runner obtained through the simulation and estimated values are shown in Figure 13. For element 2, error recorded was 4.77% and 4.16% for element 5. Figures 14 and 15 show the estimated and the simulated flow rate values at two elements, elements 2 and 5 respectively.

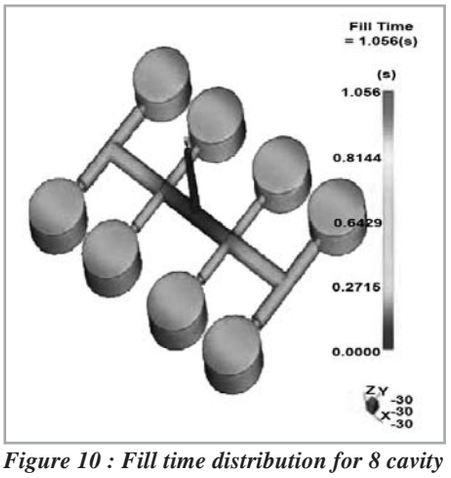

Figure 10 : Fill time distribution for 8 cavity traditional runner

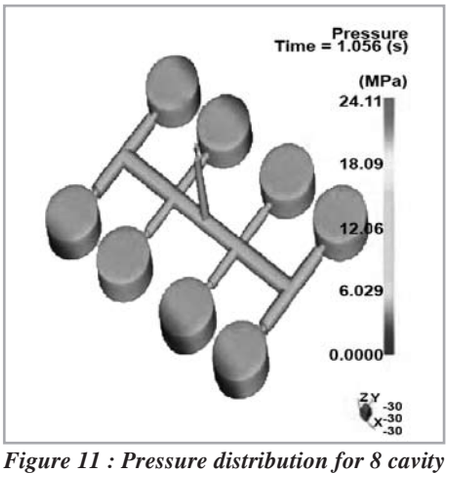

Figure 11 : Pressure distribution for 8 cavity traditional runner

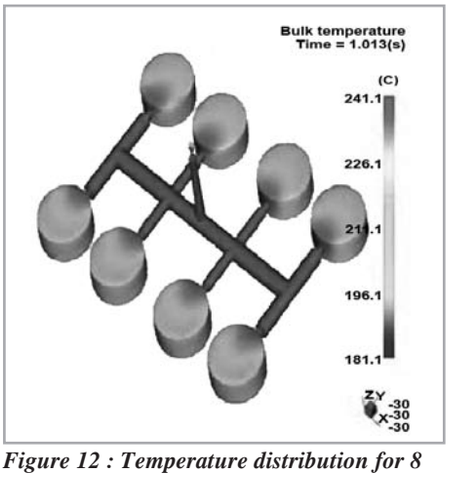

Figure 12 : Temperature distribution for 8 cavity traditional runner

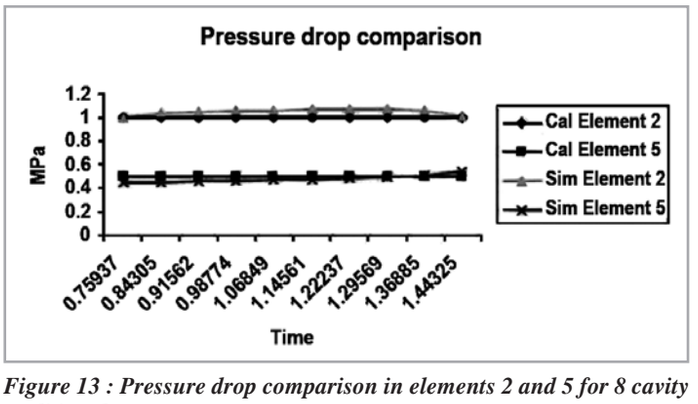

Figure 13 : Pressure drop comparison in elements 2 and 5 for 8 cavity traditional runner

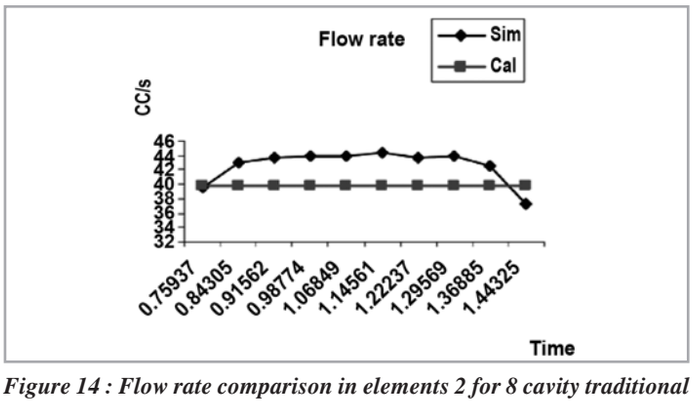

Figure 14 : Flow rate comparison in elements 2 for 8 cavity traditional runner

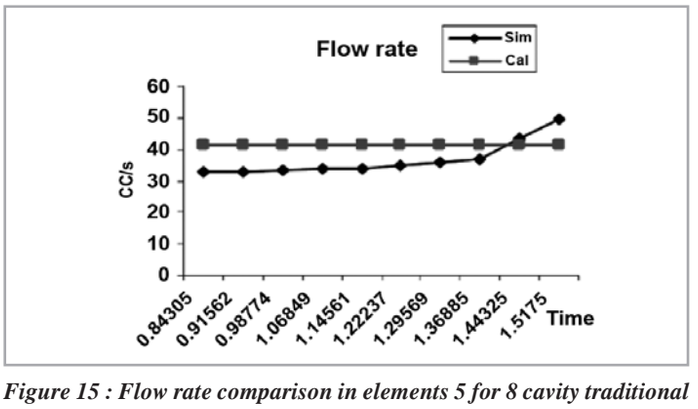

Figure 15 : Flow rate comparison in elements 5 for 8 cavity traditional runner

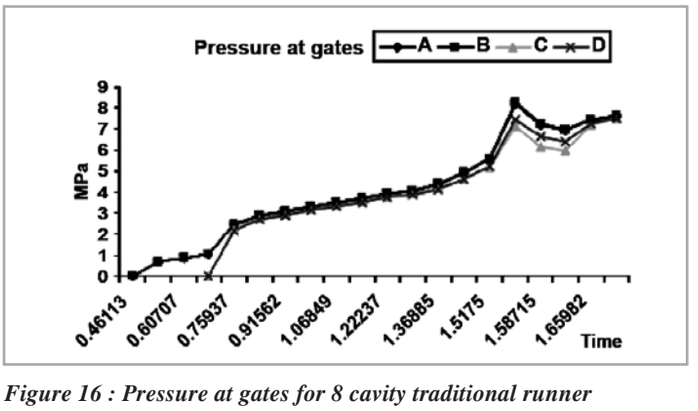

Figure 16 : Pressure at gates for 8 cavity traditional runner

The error recorded for the melt flow rate at elements 2 was 6.42% and for element 5 was 11.73%. Figure 16, meanwhile shows the pressure distribution at gates A, B, C and D.

4.2 RESULTS FOR 16 CAVITY TRADITIONAL RUNNER

4.2.1 SIMULATION FOR 16 CAVITY RUNNER

In this simulation, a traditional type of runner layout was used. The cavity is placed at a desired position inside the mold with distance that has been derived using values from Table 2.

Table 2: Parameters for 16 cavity traditional runner

	Elements			
	1	**2**	**4**	**5**
$P_{initial}$ (MPa)	6	5.5	5.5	5
P_{final} (MPa)	5.5	3.5	5	3.5
P_{drop} (MPa)	0.5	2	0.5	1.5
Radius (m)	0.0058	0.0021	0.0067	0.0024
Length (m)	0.03	0.03	0.05	0.03
$T_{initial}$ (°C)	240	243.64	243.64	242.34
T_{final} (°C)	243.64	253.43	242.34	248.09
Time step (sec)	0.5	0.5	0.5	0.5
Mesh size (m)	0.008	0.008	0.008	0.008
No. of element	3.75	3.75	6.25	3.75
Element time-step	0.133	0.133	0.08	0.133
η (°C)	233.864	220.922	220.922	225.458
Flow rate (m^3/s)	9.80E-05	1.09E-05	7.85E-05	1.13E-05
Flow rate (cc/s)	98.026	10.846	78.494	11.335

	Elements			
	7	**8**	**10**	**11**
$P_{initial}$ (MPa)	5	4.5	4.5	4
P_{final} (MPa)	4.5	3.5	4	3.5
P_{drop} (MPa)	0.5	1	0.5	0.5
Radius (m)	0.0058	0.0028	0.0052	0.0037
Length (m)	0.05	0.03	0.05	0.03
$T_{initial}$ (°C)	242.34	241.52	241.52	241.06
T_{final} (°C)	241.52	243.81	241.06	241.31
Time step (sec)	0.5	0.5	0.5	0.25
Mesh size (m)	0.008	0.008	0.008	0.008
No. of element	6.25	3.75	6.25	3.75
Element time-step	0.08	0.133	0.08	0.067
η (°C)	225.458	228.359	228.359	230.005
Flow rate (m^3/s)	3.85E-05	1.05E-05	2.27E-05	1.09E-05
Flow rate (cc/s)	38.516	10.517	22.712	10.925

Using the same boundary condition, it was found that equal filling has been achieved in all the three desired parameters of fill time, pressure and temperature. Figure 17 shows runner layout with numbered element, nodes and gates.

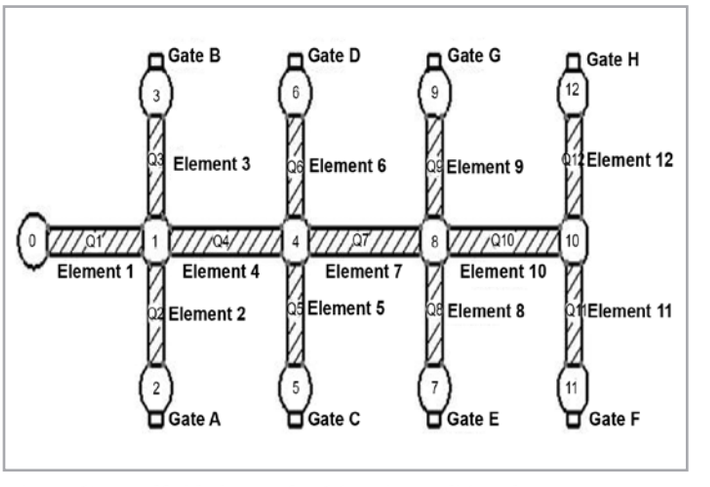

Figure 17 : Half side layout for 16 cavity traditional runner

4.2.2 MELT FLOW PATH FOR 16 CAVITY RUNNER

Figure 18 shows the result of fill time for traditional 16 cavity runner. The pressure distribution for the same 16 cavity runner is shown in Figure 19 while the temperature distribution is shown in Figure 20.

A similar plot of colors was again observed in Figures 18, 19 and 20; similar to the observation made on the 8 cavity runner earlier on. This observation indicated, again, that equal fill time, pressure and temperature were achieved. When comparing the simulated and calculated results of the pressure drop at each element leading to the gate, as shown in Figure 21, errors for elements 2, 5, 8 and 11 were considerably low, at 6.83%, 3.36%, 1.23% and 1.23% respectively.

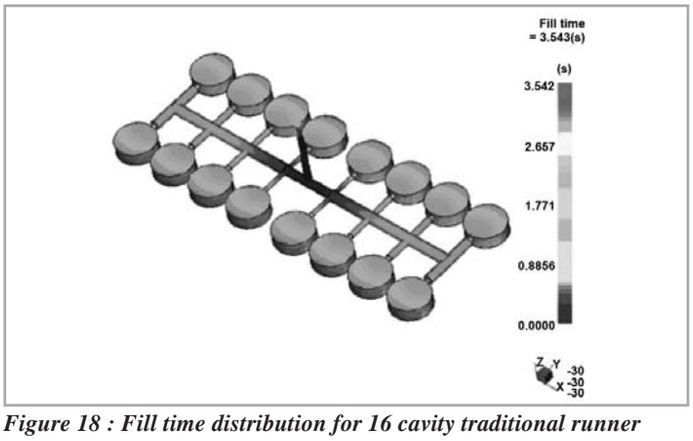

Figure 18 : Fill time distribution for 16 cavity traditional runner

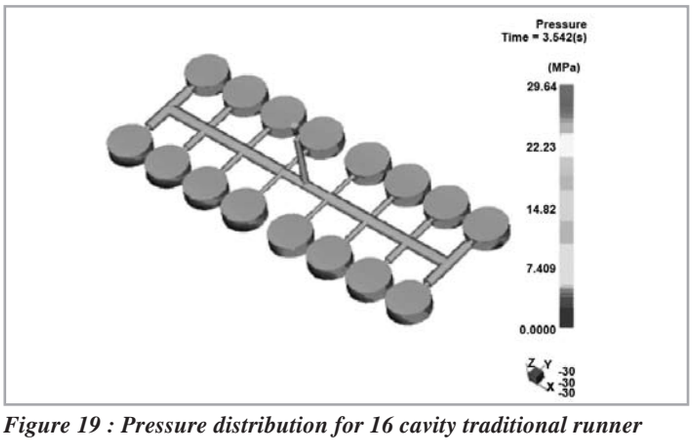

Figure 19 : Pressure distribution for 16 cavity traditional runner

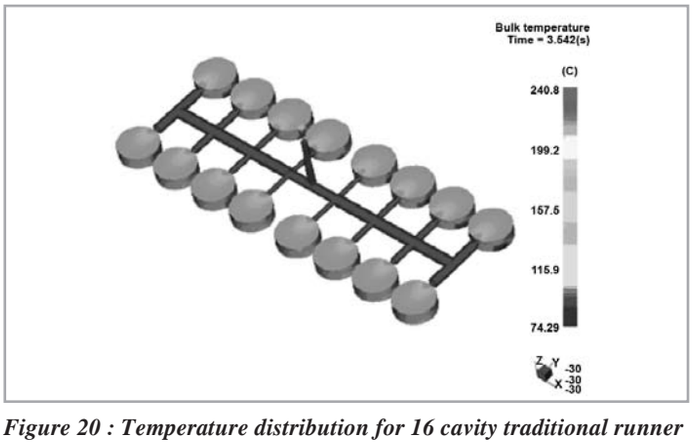

Figure 20 : Temperature distribution for 16 cavity traditional runner

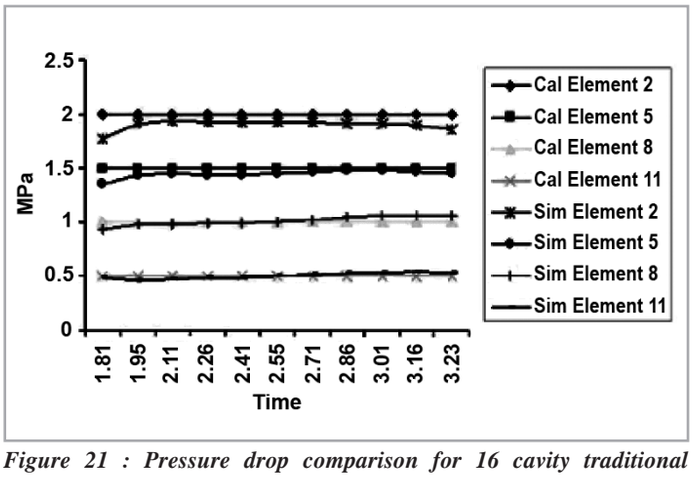

Figure 21 : Pressure drop comparison for 16 cavity traditional runner

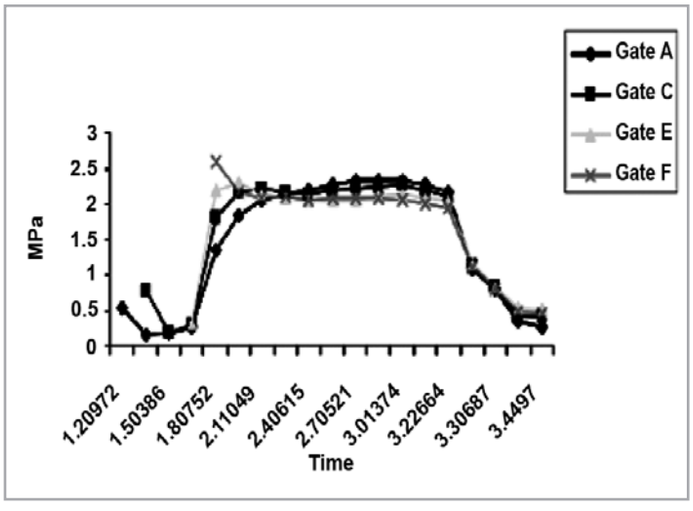

Figure 22 : Pressure at each gates for 16 cavity traditional runner

At the same time, an almost identical value of pressure distribution at each gate throughout the filling process, as indicated in Figure 22.

The calculated and simulated flow rate values in the elements leading to each gate are shown in Figure 23 (for element 2), Figure 24 (for element 5), Figure 25 (for element 8) and Figure 26 (for element 11). The observed error was noted to be low at 4.50%, 4.93%, 0.96% and 4.62 % for elements 2, 4, 8 and 11 respectively.

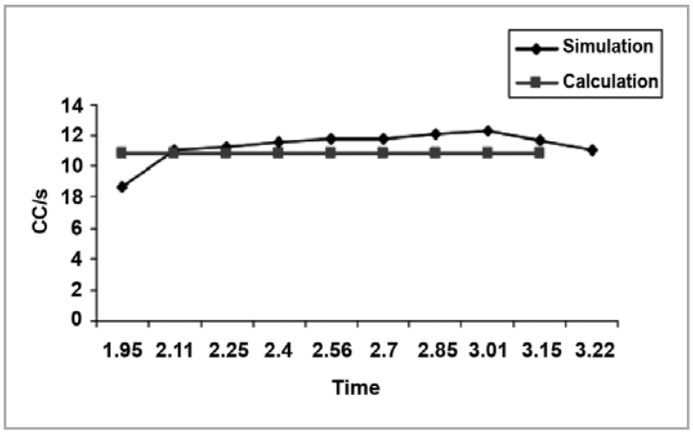

Figure 23 : Flow rate comparison in element 2 for 16 cavity traditional runner

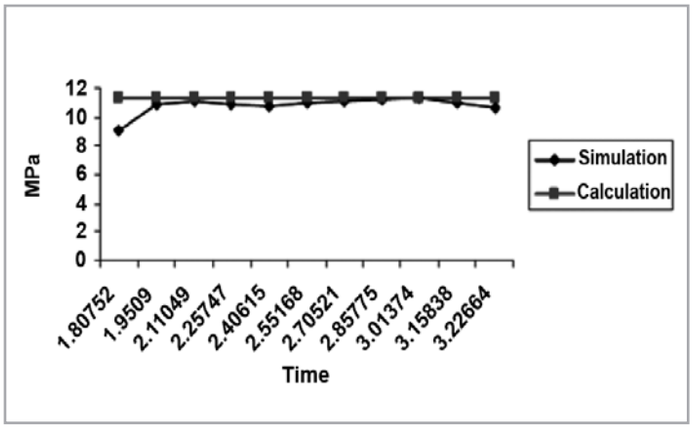

Figure 24 : Flow rate comparison in element 5 for 16 cavity traditional runner

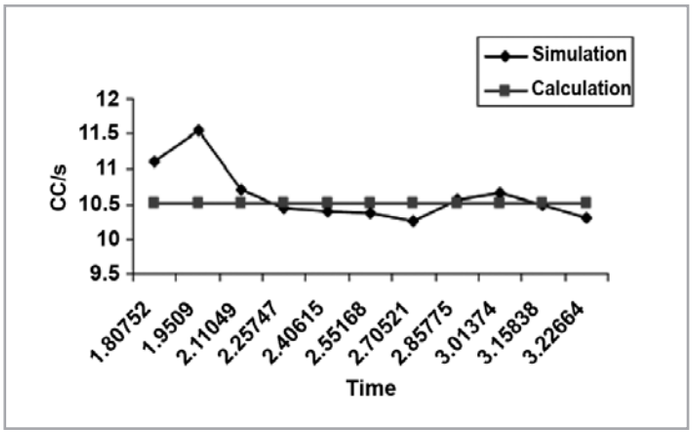

Figure 25 : Flow rate comparison in elements 8 for 16 cavity traditional runner

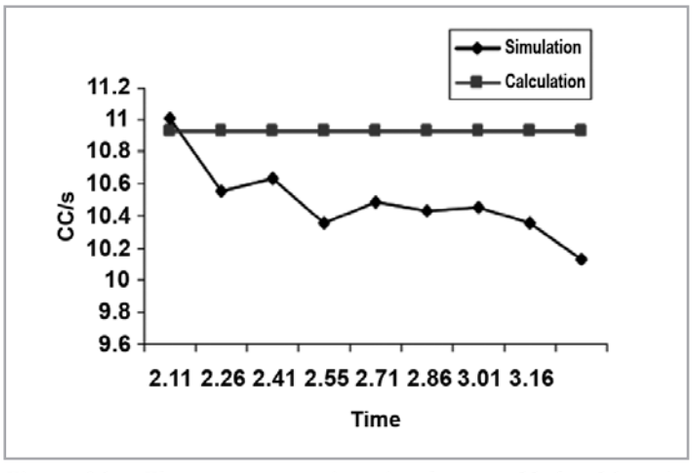

Figure 26 : Flow rate comparison in elements 11 for 16 cavity traditional runner

4.3 RESULTS FOR 8 CAVITY H-BRANCHING RUNNER

4.3.1 SIMULATION FOR 8 CAVITY RUNNER

In this simulation, *H*-branching type of runner layout was used. This type of runner is different to the one that has been discussed earlier on. This type of runner actually split the flow twice if compared to the single flow within a traditional runner layout. Figure 27 shows the runner layout with numbered elements, nodes and gates.

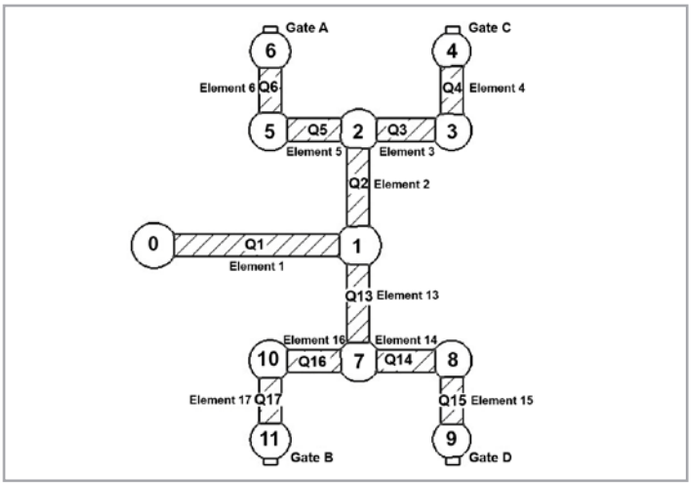

Figure 27 : Half side layout for 8 cavity H-branching runner

Results of fill time, pressure and temperature distribution for *H*-branching 8 cavity runner are shown in Table 3. In the pressure flow path, one of the cavity shows low pressure at the end of the filling while in temperature and fill time flow path, all cavities show equal filling capacity. The ratio between each element to gate is taken as the measuring index.

Table 3: Parameters for 8 cavity H-branching runner

	Elements					
	1	**2**	**3**	**4**	**5**	**6**
$P_{initial}$ (MPa)	6	5	4.5	4	4.5	4.25
P_{final} (MPa)	5	4.5	4	3	4.25	3
P_{drop} (MPa)	1	0.5	0.5	1	0.25	1.25
Radius (m)	0.005	0.004	0.003	0.0027	0.0039	0.0024
Length (m)	0.05	0.03	0.02	0.03	0.02	0.03
$T_{initial}$ (°C)	240	244.04	242.47	242.51	242.47	241.25
T_{final} (°C)	244.04	242.47	242.51	243.8	241.25	244.5
Time step (sec)	0.5	0.5	0.5	0.5	0.5	0.5
Mesh size	0.008	0.008	0.008	0.008	0.01	0.01
No. of element	6.25	3.75	2.5	3.75	2.5	3.75
Element time-step	0.08	0.133	0.2	0.133	0.2	0.13
η (°C)	233.864	219.555	225.012	224.861	225.01	229.33
Flow rate (m^3/s)	6.73E-05	1.67E-05	8.54E-06	8.90E-06	8.73E-06	7.59E-06
Flow rate (cc/s)	67.323	16.654	8.543	8.9	8.73	7.59

4.3.2 MELT FLOW PATH FOR 8 CAVITY RUNNER

Figure 28 shows the simulation results of fill time for the 8 cavity runner. The simulated result for the pressure drop is shown in Figure 29, meanwhile Figure 30 shows the temperature distribution.

While satisfactory filling occurs for fill time and temperature, it is shown in Figure 29 that one of the cavities has smaller pressure at the end of fill. In order to show the differences between the calculated and simulated results for H-branching runner, comparison will be made through the ratio of element leading to gate at each branch. This was performed because flow rate is divided into two parts. Ratio comparison produced more acceptable results. Figure 31 shows the ratio of pressure drop between elements 4 and 6 while Figure 32 show the flow rate between elements 4 and 6. Error recorded for ratio of pressure drop is 8.474% and for the flow rate at 3.56%. The pressure at each gate is shown in Figure 33.

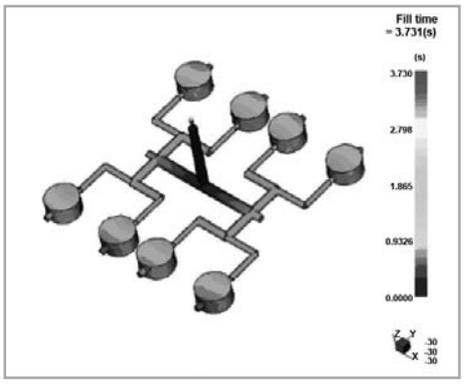

Figure 28 : Fill time distribution for 8 cavity H-branching runner

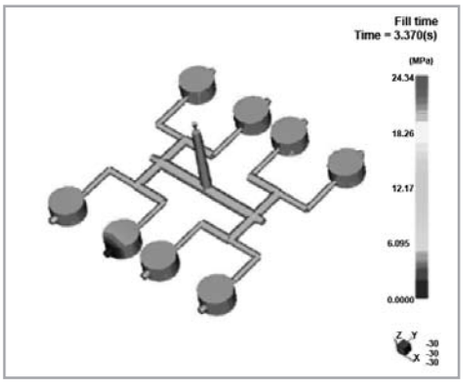

Figure 29 : Pressure drop distribution for 8 cavity H-branching runner

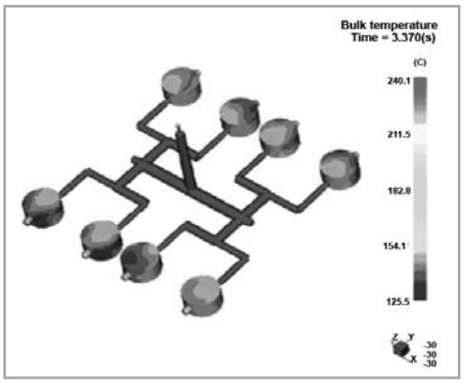

Figure 30 : Temperature distribution for 8 cavity H-branching runner

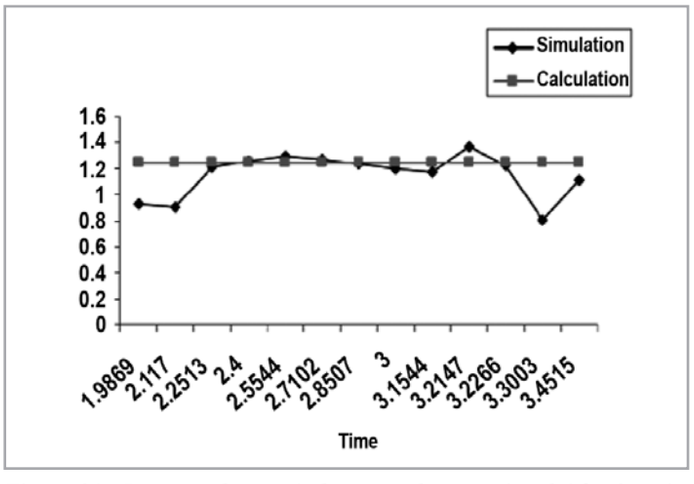

Figure 31 : Pressure drop ratio between elements 4 and 6 for 8 cavity H-branching runner

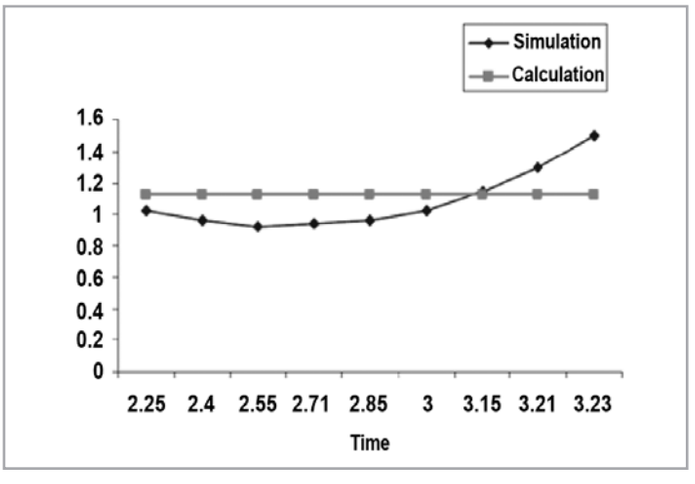

Figure 32 : Flow rate ratio between elements 4 and 6 for 8 cavity H-branching runner

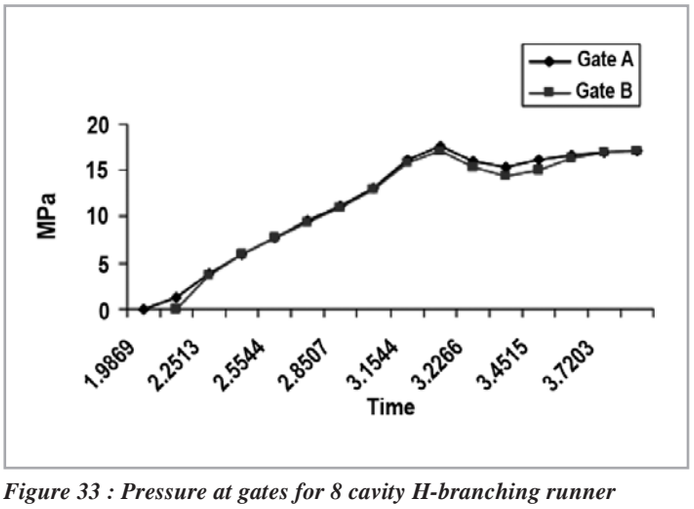

Figure 33 : Pressure at gates for 8 cavity H-branching runner

4.4 RESULTS FOR 16 CAVITY H-BRANCHING RUNNER

4.4.1 SIMULATION OF 16 CAVITY RUNNER

This runner layout is an extension of the 8 cavity runner simulated earlier. As shown in Figure 34, it also has the feature of traditional runner layout, where the flow rate in primary runner is divided into two secondary runners. This runner has the largest number of element. Therefore, in the estimation process, it is required for users to follow the melt flow rate distribution rules discussed earlier. In the simulation results, it was found that equal cavity fillings has been achieved at all but one cavity, where at this cavity there is a slightly lower pressure at the end of the filling.

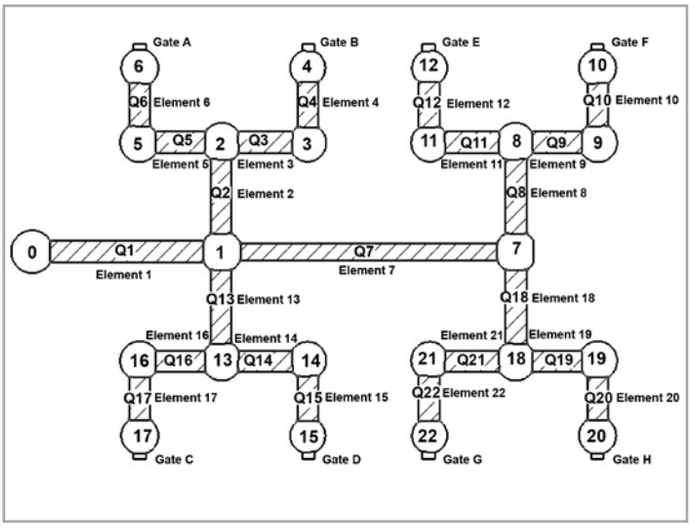

Figure 34 : Half side layout for 16 cavity H-branching runner

4.4.2 MELT FLOW PATH FOR 16 CAVITY RUNNER

Figure 35 shows the result of fill time for 16 cavity H-branching runner. The pressure distribution result for the same configuration is shown in Figure 36 and temperature distribution shown in Figure 37. At each gate, it was observed that similar color was plotted indicating an equal fill time and temperature has been achieved. However, on the flow path, it was seen that one of the cavities has slightly lower pressure compared to the others.

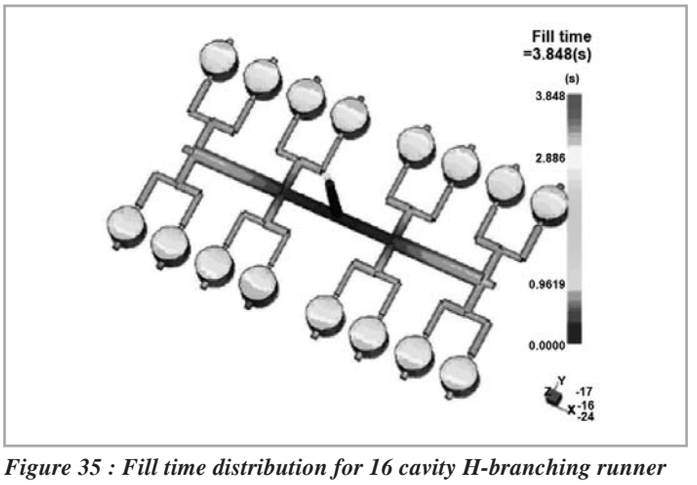

Figure 35 : Fill time distribution for 16 cavity H-branching runner

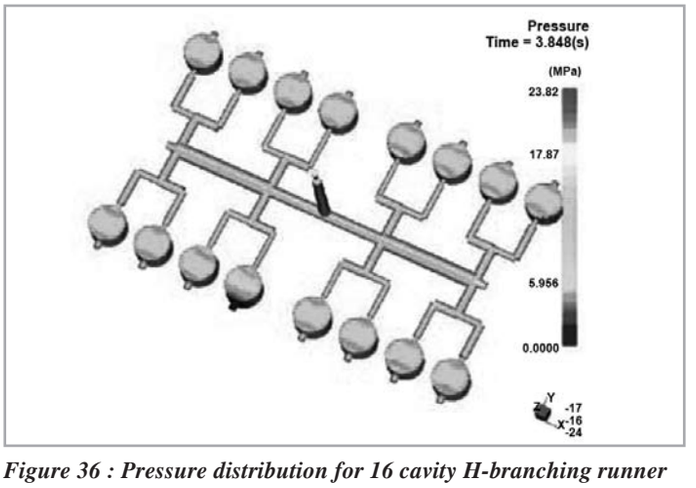

Figure 36 : Pressure distribution for 16 cavity H-branching runner

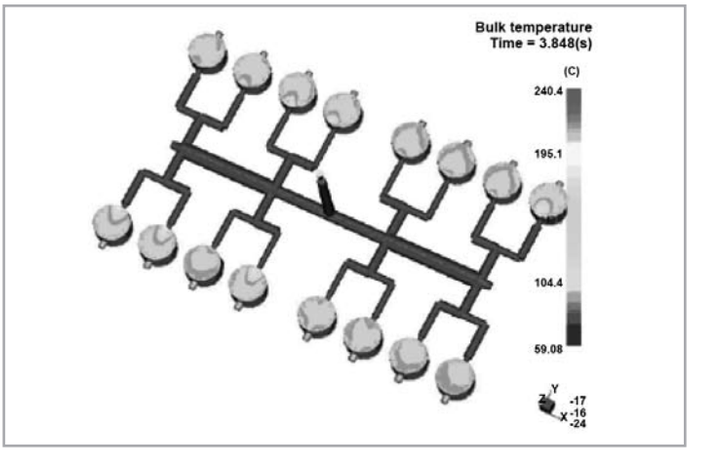

Figure 37: Temperature distribution for 16 cavity H-branching runner

Figure 38 shows the calculated and simulated ratio of pressure drop between elements 4 and 6, and elements 10 and 12. Errors recorded were 5.476% and 2.214% respectively. Figure 39 shows the ratio of flow rate element between elements 4 and 6 and Figure 40 shows the ratio of flow rate between elements 10 and 12.

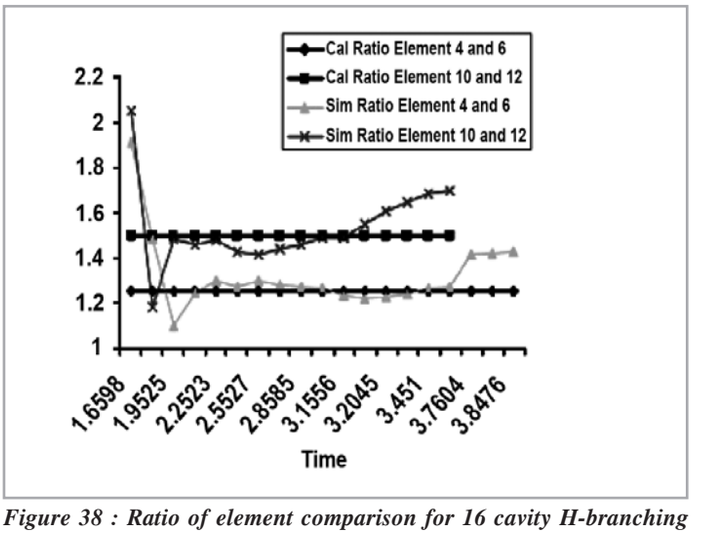

Figure 38 : Ratio of element comparison for 16 cavity H-branching runner

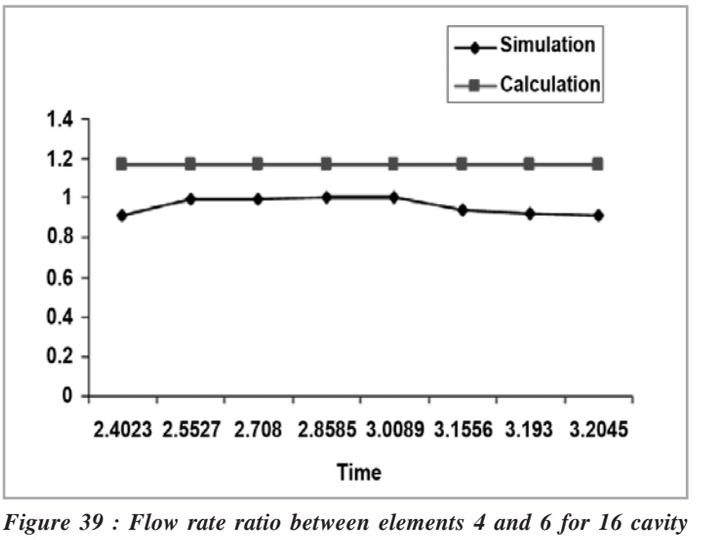

Figure 39 : Flow rate ratio between elements 4 and 6 for 16 cavity H-branching runner

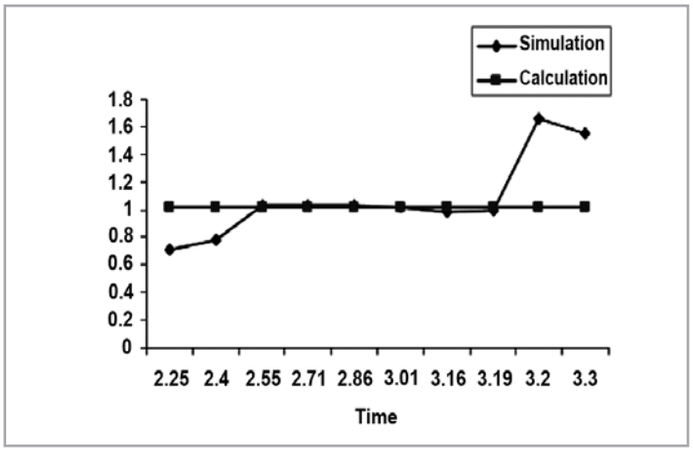

Figure 40 : Flow rate ratio between element 10 and 12 for 16 cavity H-branching runner

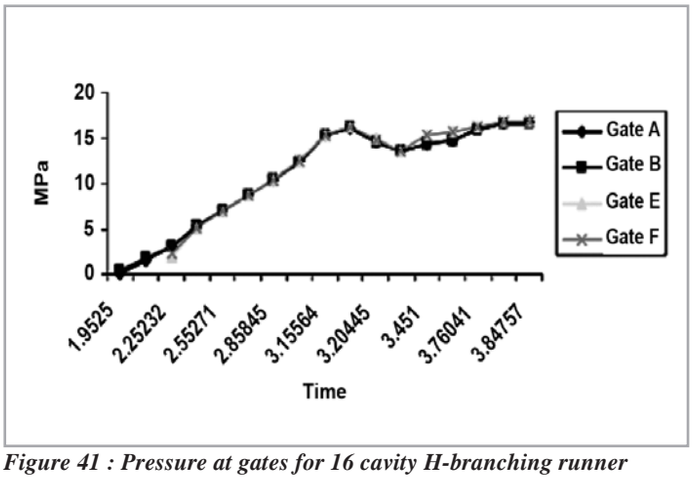

Figure 41 : Pressure at gates for 16 cavity H-branching runner

The errors when comparing the calculated and simulated ratio of flow rate between elements 4 and 6 was 9.7%, while the error for the ratio of flow rate between elements 10 and 12 was 5.14%. An equal pressure at each gate for this configuration was still observed as shown in Figure 41.

4.5 DISCUSSIONS

Overall, both the predicted parameters obtained from calculation and the values produced by MoldFLow analysis were in general agreement. However, there were few departures of values such as at the initial and final values of the flow rate, shown in Figures 15, 25, 31, 38 and 40. These were due to the adoption of different viscosity models by both techniques employed; the calculations were based on Ellis Model while the MoldFLow analysis employs the cross WLF model.

4.5.1 TRADITIONAL RUNNER LAYOUT

The described calculation technique discussed earlier was compared against values obtained from the Moldflow software with the assumed parameters in the listed table for each case. Each cavity is situated 30-mm from the mold center. Pressure measurement at each gate was also obtained. The predicted melt flow path was also shown to provide an insight of what actually happened in the injection process. From the inlet, melt flow freely into the first branch and separated into three parts. When considering an 8 cavity mold in section 4.1, as an example, the melt filled the cavity in the first branch first before filling into the next branch. On the first branch, the melt flow into element 2 at 0.188s and reached the end of the element at 0.4249s, at which, at the same time, the melt would then flow into element 5. At this point, since equation 11 is in viscosity terms of shear stress and shear rate, it was found that shear stress at the wall in element 2 was larger than those in element 5.

Referring to Table 1, although the flow rate was equal but the diameter of element 5 at 98 cm was significantly larger than the element 2 diameter of 74 cm. Therefore, at gate A, only small volume of melt appears to trickle into the cavity, while waiting for element 5 to be fully-filled. Once element 5 is fully-filled, only then will the melt flow in continuously at an equal flow rate. The calculated and simulated values start exactly at the time when the two elements have been filled. Therefore it satisfies equation 13 that compensate for runner wall temperature. Wall temperature for this condition was assumed at 240°C which mean the melt doesn't experience temperature drop at the wall. For the 8 cavity mold, at element 2, the shear stress was 0.0363MPa and the shear rate was 52.86/s. In element 5, the shear stress and shear rate is at 0.0184MPa and 16.19/s respectively.

4.5.2 H-BRANCHING RUNNER LAYOUT

One problem that has been perceived is that the cause of filling imbalance is mainly due to the flow imbalance between the cavities when there are non-uniform material properties entering into each cavity. Figure 42 can help to clarify this claim.

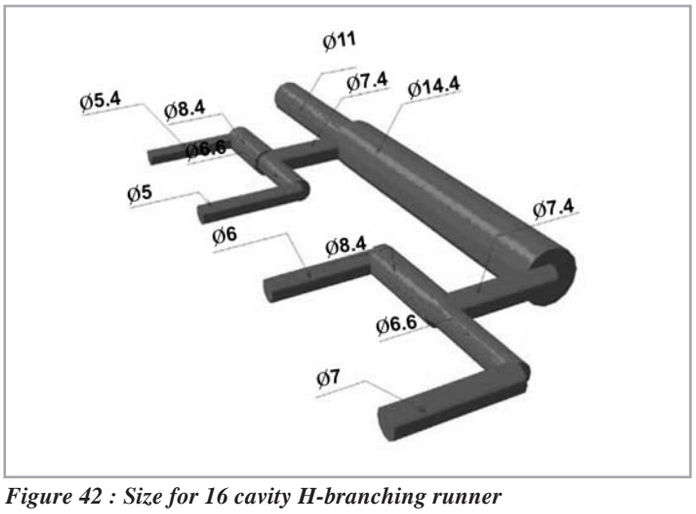

Figure 42 : Size for 16 cavity H-branching runner

In a mold with a single branch in the runner, the velocity, shear rate, temperature, and viscosity distribution across the branching runner will become non-symmetrical from side to side in the secondary runner. The hotter outer laminates on one side of the primary runner will flow along the left wall of the secondary runner. The cooler center laminates will go to the opposite right side of the secondary runner. Similarly, the hotter outer laminates at the bottom portion of the primary runner will follow along the wall of the left side of tertiary runner. The cooler center laminates will go to the opposite right edge of tertiary runner. One half of the secondary runner will be hotter than the other half. Therefore, using this technique molders can control the variation in flow rate and shear distribution inside the branched runner. Table 4 shows, almost identical melt flow rate are set at element leading to the gate. Thus, by having equal flow rate, the melt is "forced" to have desired shear rate and shear stress, stimulated by runner diameter and length.

Table 4: Parameters for 16 cavity H-branching runner

	Elements					
	1	**2**	**3**	**4**	**5**	**6**
$P_{initial}$ (MPa)	6	5	4.5	4	4.5	4.25
P_{final} (MPa)	5	4.5	4	3	4.25	3
p_{drop} (MPa)	1	0.5	0.5	1	0.25	1.25
Radius (m)	0.005	0.004	0.003	0.0027	0.0039	0.0024
Length (m)	0.05	0.03	0.02	0.03	0.02	0.03
$T_{initial}$ (°C)	240	244.04	242.47	242.51	242.47	241.25
T_{final} (°C)	244.04	242.47	242.51	243.8	241.25	244.5
Time step (sec)	0.5	0.5	0.5	0.5	0.5	0.5
Mesh size	0.008	0.008	0.008	0.008	0.01	0.01
No. of element	6.25	3.75	2.5	3.75	2.5	3.75
Element time-step	0.08	0.133	0.2	0.133	0.2	0.13
η (°C)	233.864	219.555	225.012	224.861	225.01	229.33
Flow rate (m^3/s)	6.73E-05	1.67E-05	8.54E-06	8.90E-06	8.73E-06	7.59E-06
Flow rate (cc/s)	67.323	16.654	8.543	8.9	8.73	7.59

	Elements					
	7	**8**	**9**	**10**	**11**	**12**
$P_{initial}$ (MPa)	5	4.5	4	3.5	4	3.75
P_{final} (MPa)	4.5	4	3.5	3	3.75	3
P_{drop} (MPa)	0.5	0.5	0.5	0.5	0.25	0.75
Radius (m)	0.0066	0.004	0.003	0.004	0.0039	0.003
Length (m)	0.08	0.03	0.02	0.03	0.02	0.03
$T_{initial}$ (°C)	244.04	241.499	241.683	242.256	241.683	241.019
T_{final} (°C)	241.5	241.68	242.26	241.53	241.02	242.04
Time step (sec)	0.5	0.5	0.5	0.5	0.5	0.5
Mesh size	0.01	0.01	0.01	0.01	0.01	0.01
No. of element	10	3.75	2.5	3.75	2.5	3.75
Element time-step	0.05	0.13	0.2	0.13	0.2	0.13
η (°C)	219.56	228.44	227.79	225.76	227.79	230.17
Flow rate (m^3/s)	3.32E-05	1.60E-05	8.44E-06	8.54E-06	8.63E-06	8.35E-06
Flow rate (cc/s)	33.18	16.01	8.44	8.54	8.63	8.35

5.0 CONCLUSIONS

An Ellis model with Arrhenius temperature dependence has four coefficients, and the Cross model with WLF temperature dependence has six coefficients. As the number of model coefficients increases, it is easier to model the melts recital. However, the increased number of model coefficients significantly increases the analysis time. This approach is to assume Ellis Viscosity model

with temperature dependence for a given material. Added to flow rate with Ellis model relationship, a number of estimations can be made in the feed system of injection molding. This thereby reduce the number of rheological parameters *e.g.* the Newtonian limit and the critical shear stress.

The results have shown, especially for pressure in elements, that molders can predict and control the shape and size requirements of molds in order to achieve the required parameter at the entrance of the gate. Initial pressure at the inlet was not that important; in that any values depending on number of cavity can be used. This was true given that larger number of cavity requires larger injection pressure. Flow rate at each element entering the gate, must be equal so that, it can achieve the required pressure drop. From all these constraints, size of runner length and diameter can be adjusted to achieve the desired results. These findings concur with the works of Lin and Tai, Sulaiman and Keen, and Hu *et. al.*, all indicating that runners do play a significant role in the mold design exercise [2,3,4].

In conclusion, the runner sizing general formula for a traditional runner layout for 8 to 20 cavities can then be described as:

For n cavity with m branches, the flow-rate at primary runner

$$Q_1 \approx Q_{(y+2m-2)}$$

Where, $y = \frac{n}{4}$

Then, $\frac{1}{2} Q_{y+2m-2} \approx Q_2 \approx Q_5 \approx Q_8 \approx Q_{11} \approx Q_{14}$

and Q_{y+2m-2} is the last element on the primary runner

While the runners sizing general formula for an H-branching runner layout with 16 cavities yield the flow-rate at runners as:

$$Q_1 = 4Q_2 \qquad Q_1 = 2Q_7$$
$$Q_2 = 2Q_3 = 2Q_5 \qquad Q_8 = 2Q_9 = 2Q_{11}$$
$$Q_3 = Q_4 = Q_5 = Q_6 \qquad Q_9 = Q_{10} = Q_{11} = Q_{12}$$

This paper has also shown that, similar to the works of Zhao *et. al.*, Lee and Lin, Fan *et. al.* and Kumar *et. al.*, [5, 6, 7, 8] that the simulation techniques and calculations performed during a mold design process is helpful in producing better molds. It is also proven that the better runner configuration to be adopted is the H-branching runner layout configuration. ■

REFERENCES

[1] M. Zhai, Y. C. Lam and C. K. Au, "Runner sizing and weld line positioning for plastics injection molding with multiple gates", *Engineering with Computers*, Vol. 21, No. 3, pp. 218-224, May, 2006.

[2] J. C. Lin and C. C. Tai, "The Runner Optimization Design of a Die-Casting Die and the Part Produced", *International Journal of Advance Manufacturing Technology*, Vol. 14, No. 2, pp. 133-145, Feb, 1998.

[3] S. Sulaiman and T.C. Keen, "Flow analysis along the runner and gating system of a casting process", *Journal of Materials Processing Technology*, Vol. 63, No. 1-3, pp. 690-695, Jan, 1997.

[4] B. H. Hu, K. K. Tong, X. P. Niu and I. Pinwill, "Design and optimisation of runner and gating systems for the die casting of thin-walled magnesium telecommunication parts through numerical simulation", *Journal of Materials Processing Technology*, Vol. 105, No. 1-2, pp. 128-133, Sep, 2000.

[5] B. Zhao, S.P. Vanka and B.G. Thomas, "Numerical study of flow and heat transfer in a molten flux layer", *International Journal of Heat and Fluid Flow*, Vol. 26, No. 1, pp. 105-118, Feb, 2005.

[6] K.S. Lee and J.C. Lin, "Design of the runner and gating system parameters for a multi-cavity injection mould using FEM and neural network", *The International Journal of Advanced Manufacturing Technology*, Vol. 27, No. 11-12, pp. 1089-1096, Feb, 2006.

[7] B. Fan, D. Kazmer and R. Mukhari, "Real Time Flow Rate Estimation in Injection Molding", *Molding Technology Symposium at the 20th Annual Meeting of the Polymer Processing Society*, Akron, OH, June, 2003.

[8] A. Kumar, P. S. Ghoshdastidar and M. K. Muju, "Computer simulation of transport processes during injection mold-filling and optimization of the molding conditions", *Journal of Materials Processing Technology*, Vol. 120, No. 1-3, pp. 438-449, Jan, 2002.

[9] D. O. Kazmer, "Professor David Kazmer for Plastic Part Design and Manufacturing", *WebMaster Mag.*, [Online]. Website: http://kazmer.uml.edu/, Oct. 21, 2005.